Immune Netw. 2024 Apr;24(2):e7
https://doi.org/10.4110/in.2024.24.e7
pISSN 1598-2629·eISSN 2092-6685

IMMUNE NETWORK

Original Article

Check for updates

Immune Cells Are Differentially Affected by SARS-CoV-2 Viral Loads in K18-hACE2 Mice

Jung Ah Kim [1,†], **Sung-Hee Kim** [2,†], **Jeong Jin Kim** [2,†], **Hyuna Noh** [3,†], **Su-bin Lee** [4], **Haengdueng Jeong** [2], **Jiseon Kim** [2], **Donghun Jeon** [2], **Jung Seon Seo** [2], **Dain On** [3,5], **Suhyeon Yoon** [3], **Sang Gyu Lee** [6], **Youn Woo Lee** [7], **Hui Jeong Jang** [7], **In Ho Park** [2,8], **Jooyeon Oh** [9], **Sang-Hyuk Seok** [10], **Yu Jin Lee** [10], **Seung-Min Hong** [11], **Se-Hee An** [11], **Joon-Yong Bae** [12], **Jung-ah Choi** [13], **Seo Yeon Kim** [14], **Young Been Kim** [14], **Ji-Yeon Hwang** [14], **Hyo-Jung Lee** [15], **Hong Bin Kim** [16], **Dae Gwin Jeong** [17], **Daesub Song** [18], **Manki Song** [13], **Man-Seong Park** [12], **Kang-Seuk Choi** [11], **Jun Won Park** [10], **Jun-Won Yun** [19], **Jeon-Soo Shin** [2,8,9], **Ho-Young Lee** [7,20], **Ho-Keun Kwon** [4], **Jun-Young Seo** [2,*], **Ki Taek Nam** [2,*], **Heon Yung Gee** [1,*], **Je Kyung Seong** [3,5,6,21,*]

[1]Department of Pharmacology, Graduate School of Medical Science, Brain Korea 21 Project, Yonsei University College of Medicine, Seoul 03722, Korea
[2]Department of Biomedical Sciences, Graduate School of Medical Science, Brain Korea 21 Project, Yonsei University College of Medicine, Seoul 03722, Korea
[3]Korea Mouse Phenotyping Center, Seoul National University, Seoul 08826, Korea
[4]Department of Microbiology and Immunology and Brain Korea 21 PLUS Project for Medical Sciences, Yonsei University College of Medicine, Seoul 03722, Korea
[5]Laboratory of Developmental Biology and Genomics, Research Institute for Veterinary Science, and BK21 PLUS Program for Creative Veterinary Science Research, College of Veterinary Medicine, Seoul National University, Seoul 08826, Korea
[6]Interdisciplinary Program for Bioinformatics, Seoul National University, Seoul 08826, Korea
[7]Department of Nuclear Medicine, Seoul National University Bundang Hospital, Seongnam 23488, Korea
[8]Institute of Immunology and Immunological Diseases, Yonsei University College of Medicine, Seoul 03722, Korea
[9]Department of Microbiology, Yonsei University College of Medicine, Seoul 03722, Korea
[10]Division of Biomedical Convergence, College of Biomedical Science, Kangwon National University, Chuncheon 24342, Korea
[11]Laboratory of Avian Diseases, BK21 PLUS Program for Veterinary Science and Research Institute for Veterinary Science, College of Veterinary Medicine, Seoul National University, Seoul 08826, Korea
[12]Department of Microbiology, Institute for Viral Diseases, Biosafety Center, Korea University College of Medicine, Seoul 02842, Korea
[13]Science Unit, International Vaccine Institute, Seoul 08826, Korea
[14]Preclinical Research Center, Seoul National University Bundang Hospital, Seongnam 23488, Korea
[15]Department of Periodontology, Section of Dentistry, Seoul National University Bundang Hospital, Seongnam 23620, Korea
[16]Department of Internal Medicine, Seoul National University Bundang Hospital, Seoul National University College of Medicine, Seongnam 23620, Korea
[17]Bionanotechnology Research Center, Korea Research Institute of Bioscience and Biotechnology, Daejeon 34242, Korea
[18]Department of Veterinary Medicine Virology Laboratory, College of Veterinary Medicine and Research Institute for Veterinary Science, Seoul National University, Seoul 08826, Korea
[19]Laboratory of Veterinary Toxicology, College of Veterinary Medicine, Seoul National University, Seoul 08826, Korea
[20]Department of Nuclear Medicine, Seoul National University, College of Medicine, Seoul 03080, Korea
[21]BIO-MAX Institute, Seoul National University, Seoul 08826, Korea

Received: Aug 14, 2023
Revised: Jan 9, 2024
Accepted: Jan 15, 2024
Published online: Feb 2, 2024

***Correspondence to**

Je Kyung Seong
Korea Mouse Phenotyping Center, Seoul National University, 1 Gwanak-ro, Gwanak-gu, Seoul 08826, Korea.
Email: snumouse@snu.ac.kr

Heon Yung Gee
Department of Biomedical Sciences, Graduate School of Medical Science, Brain Korea 21 Project, Yonsei University College of Medicine, 50 Yonsei-ro, Seodaemun-gu, Seoul 03722, Korea.
Email: hygee@yuhs.ac

Ki Taek Nam
Department of Biomedical Sciences, Graduate School of Medical Science, Brain Korea 21 Project, Yonsei University College of Medicine, 50 Yonsei-ro, Seodaemun-gu, Seoul 03722, Korea.
Email: kitaek@yuhs.ac

Jun-Young Seo
Department of Biomedical Sciences, Graduate School of Medical Science, Brain Korea 21 Project, Yonsei University College of Medicine, 50 Yonsei-ro, Seodaemun-gu, Seoul 03722, Korea.
Email: jyseo0724@yuhs.ac

†Jung Ah Kim, Sung-Hee Kim, Jeong Jin Kim, and Hyuna Noh were equally contributed as first authors.

ORCID iDs
Jung Ah Kim
https://orcid.org/0000-0002-1264-8328
Sung-Hee Kim
https://orcid.org/0000-0002-2970-9449
Jeong Jin Kim
https://orcid.org/0000-0002-8886-5441
Hyuna Noh
https://orcid.org/0000-0003-4806-6730
Su-bin Lee
https://orcid.org/0009-0001-8023-5613
Haengdueng Jeong
https://orcid.org/0000-0002-9218-7372
Jiseon Kim
https://orcid.org/0000-0002-0979-0278
Donghun Jeon
https://orcid.org/0000-0002-9161-6198
Jung Seon Seo
https://orcid.org/0000-0001-6238-6023
Dain On
https://orcid.org/0000-0002-6227-2058
Suhyeon Yoon
https://orcid.org/0000-0002-3883-8330
Sang Gyu Lee
https://orcid.org/0000-0001-5719-4035
Youn Woo Lee
https://orcid.org/0000-0002-4559-1604
Hui Jeong Jang
https://orcid.org/0000-0003-2019-6269
In Ho Park
https://orcid.org/0000-0003-2190-5469
Jooyeon Oh
https://orcid.org/0000-0003-1701-7792
Sang-Hyuk Seok
https://orcid.org/0000-0002-9213-8706
Yu Jin Lee
https://orcid.org/0000-0002-6386-5381
Seung-Min Hong
https://orcid.org/0000-0001-5488-8445
Se-Hee An
https://orcid.org/0000-0002-2206-1299
Joon-Yong Bae
https://orcid.org/0000-0002-2483-4208
Jung-ah Choi
https://orcid.org/0000-0003-2381-7374
Seo Yeon Kim
https://orcid.org/0000-0001-5178-2055

ABSTRACT

Viral load and the duration of viral shedding of severe acute respiratory syndrome coronavirus 2 (SARS-CoV-2) are important determinants of the transmission of coronavirus disease 2019. In this study, we examined the effects of viral doses on the lung and spleen of K18-hACE2 transgenic mice by temporal histological and transcriptional analyses. Approximately, 1×10^5 plaque-forming units (PFU) of SARS-CoV-2 induced strong host responses in the lungs from 2 days post inoculation (dpi) which did not recover until the mice died, whereas responses to the virus were obvious at 5 days, recovering to the basal state by 14 dpi at 1×10^2 PFU. Further, flow cytometry showed that number of CD8+ T cells continuously increased in 1×10^2 PFU-virus-infected lungs from 2 dpi, but not in 1×10^5 PFU-virus-infected lungs. In spleens, responses to the virus were prominent from 2 dpi, and number of B cells was significantly decreased at 1×10^5 PFU; however, 1×10^2 PFU of virus induced very weak responses from 2 dpi which recovered by 10 dpi. Although the defense responses returned to normal and the mice survived, lung histology showed evidence of fibrosis, suggesting sequelae of SARS-CoV-2 infection. Our findings indicate that specific effectors of the immune response in the lung and spleen were either increased or depleted in response to doses of SARS-CoV-2. This study demonstrated that the response of local and systemic immune effectors to a viral infection varies with viral dose, which either exacerbates the severity of the infection or accelerates its elimination.

Keywords: SARS-CoV-2; K18-hACE2 mice; Dose-response relationship, immunologic; Transcriptome profiling; Immune response

INTRODUCTION

A cluster of pneumonia cases was reported in Wuhan, China in December 2019. The Chinese health authorities confirmed on January 7, 2020 that this cluster was associated with a novel coronavirus. The World Health Organization dubbed this novel coronavirus infection "coronavirus disease 2019" (COVID-19) on February 11 (1). The causative agent of the pandemic, known as severe acute respiratory syndrome coronavirus 2 (SARS-CoV-2), is a positive-sense, single-stranded RNA virus belonging to the family Coronaviridae (2). Upon binding to epithelial cells in the respiratory tract, SARS-CoV-2 begins replication and migration to the airways, and entry into alveolar epithelial cells (3). In a separate study, the effects of infectious SARS-CoV-2 doses on the pathology of K18-hACE2 transgenic mice were evaluated (4). According to the study, 2×10^3 plaque-forming units (PFU) or 2×10^4 PFU SARS-CoV-2 were lethal enough to kill 90% of the mice around 7 days post inoculation (dpi), while some of the mice infected with 2×10^1 PFU or 2×10^2 PFU died at 10 dpi, and the others recovered and survived until 20 dpi (4). In terms of histopathology, high-dose groups exhibited extensive alveolar collapse with ruptured septa, whereas 30%–60% of low-dose groups exhibited alveolar congestion in the alveoli (4). Nevertheless, previous studies did not investigate the effects of a viral inoculum dose on the transcriptome of an animal model (4).

Several viral infections, including influenza and SARS, have demonstrated a correlation between infectious dose and disease severity (5,6). For COVID-19, high viral loads in the saliva, respiratory secretions, and blood were associated with more severe illnesses (7,8). A previous study on SARS-CoV-2 infection in 16 cynomolgus macaques demonstrated that the infectious dose indeed influenced both symptom development and seroconversion (9). Low doses of aerosolized viruses led to seroconversion and viral replication in the respiratory

Young Been Kim
https://orcid.org/0000-0003-4838-996X
Ji-Yeon Hwang
https://orcid.org/0000-0003-4154-3012
Hyo-Jung Lee
https://orcid.org/0000-0002-4991-0705
Hong Bin Kim
https://orcid.org/0000-0001-6262-372X
Dae Gwin Jeong
https://orcid.org/0000-0002-0764-1404
Daesub Song
https://orcid.org/0000-0002-2759-1061
Manki Song
https://orcid.org/0000-0002-8279-9041
Man-Seong Park
https://orcid.org/0000-0002-7427-486X
Kang-Seuk Choi
https://orcid.org/0000-0001-6825-6924
Jun Won Park
https://orcid.org/0000-0003-4677-1786
Jun-Won Yun
https://orcid.org/0000-0002-0155-4190
Jeon-Soo Shin
https://orcid.org/0000-0002-8294-3234
Ho-Young Lee
https://orcid.org/0000-0001-6518-0602
Ho-Keun Kwon
https://orcid.org/0000-0003-3175-0376
Jun-Young Seo
https://orcid.org/0000-0003-4004-2013
Ki Taek Nam
https://orcid.org/0000-0001-5292-1280
Heon Yung Gee
https://orcid.org/0000-0002-8741-6177
Je Kyung Seong
https://orcid.org/0000-0003-1177-6958

Conflict of Interest
The authors declare no potential conflicts of interest.

Abbreviations
COVID-19, coronavirus disease 2019; DEG, differentially expressed gene; dpi, days post-inoculation; FDR, false discovery rate; GO, Gene Ontology; GSVA, gene set variation analysis; PFU, plaque-forming unit; RNA-seq, RNA-sequencing; SARS-CoV-2 severe acute respiratory syndrome coronavirus 2; TPM, transcripts per kilobase million.

Author Contributions
Conceptualization: Seo JY, Nam KT, Seong JK; Data curation: Kim JA, Kim SH, Kim JJ, Noh H; Formal analysis: Kim JA, Kim SH, Kim JJ, Noh H; Investigation: Kim JA, Kim SH, Kim JJ, Noh H, Lee SB, Jeong H, Kim J, Jeon D, Seo JS, On D, Yoon S, Lee SG, Lee YW, Jang HJ, Park IH,

tract without symptom development, whereas high doses produced fever, suggesting that low infectious doses may be associated with asymptomatic infections (9). In addition, a dose titration study of SARS-CoV-2 in a ferret model demonstrated evidence of protective immunity (10). When a high (5×10^6 PFU) or moderate (5×10^5 PFU) dose of the virus was delivered intranasally, viral RNA shedding was observed in the upper respiratory tract of all animal subjects. However, only one out of 6 ferrets exhibited comparable symptoms in response to a low-dose (5×10^2 PFU) challenge (10).

Despite previous research on the correlation between viral concentration and the manifestation of infection, it remains unclear whether exposure to a higher viral inoculum could increase the likelihood of developing severe COVID-19. Although intuitive, obtaining such dose-response data has been difficult. In addition, the immune responses to varying doses of virus infection in K18-hACE2 transgenic mice, in which hACE2 expression is controlled by the epithelial cell cytokeratin-18 (K18) promoter for efficient SARS-CoV-2 infection, are not completely understood (11-14). Therefore, in this study, we aimed to assess the overall clinical pathogenesis and transcriptome profile of the lungs and spleens of K18-hACE2 transgenic mice intranasally inoculated with 1×10^5 and 1×10^2 PFU of SARS-CoV-2. The dose-specific response to SARS-CoV-2 infection was better comprehended through a thorough examination of these organs.

MATERIALS AND METHODS

Mice and virus

This research used 8-wk-old K18-hACE2 male mice (B6.Cg-Tg[K18-ACE2]2Prlmn/J, Hemizygous, #034860; Jackson Laboratory, Bar Harbor, ME, USA) for SARS-CoV-2 infection. The protocol for animal experiments was approved by the Institutional Animal Care and Use Committee (2020-0216, BA-2008-301-071-03) of Yonsei University College of Medicine. SARS-CoV-2 (accession number: NCCP 43326, S clade, beta variant) was obtained from the National Culture Collection for Pathogens in Korea and passaged using the Vero cell line (Korean Cell Line Bank, Korea, accession number: 10081).

Infection of mice

Mice were anesthetized with 30 mg kg-1 zoletil/10 mg kg-1 rompun. Next, intranasal infection was performed with phosphate-buffered saline for mock and 1×10^2 and 1×10^5 PFU SARS-CoV-2 in 50 µl of culture medium. The infected mice were weighed and body temperature measured daily using an implantable temperature transponder (Bio Medic Data Systems, Seaford, DE, USA). Over 20% of body weight loss and 10°C of body temperature loss mouse euthanized using CO_2. All experiments with SARS-CoV-2 were conducted in the biosafety level 3 laboratory at Yonsei University College of Medicine.

Histopathological analysis

The SARS-CoV-2-infected mice were euthanized, and autopsies were conducted. The delivered tissues were fixed in 10% neutral buffered formalin for 24 h and embedded in paraffin wax. For histopathological analysis, the paraffin blocks were sectioned at 4 µm thickness, deparaffinized, and stained with H&E. The stained slides were deciphered by an animal pathologist, and lung pathological findings were categorized. Inflammation due to the infiltration of immune cells, edema, and the capillary dilatation were the main pathologies behind the lesions detected. The lesion grade, compared with control, was

Oh J, Seok SH, Lee YJ, Hong SM, An SH, Bae JY, Choi JA, Kim SY, Kim YB, Hwang JY, Lee HJ, Kim HB, Jeong DG, Song D, Song M, Park MS, Choi KS, Park JW, Yun JW, Shin JS, Lee HY, Kwon HK; Methodology: Kim JA, Kim SH, Kim JJ, Noh H; Project administration: Seo JY, Nam KT, Gee HY, Seong JK; Resources: Seo JY, Nam KT, Gee HY, Seong JK; Supervision: Seo JY, Nam KT, Gee HY, Seong JK; Validation: Kim JA, Kim SH, Kim JJ, Noh H; Writing - original draft: Kim JA, Kim SH, Gee HY; Writing- review & editing: Seo JY, Nam KT, Gee HY, Seong JK.

assessed by pathologists into 6 grades as follows: 0 (no lesions), 1 (<10% rare lesions in alveolar, endothelial and bronchus region), 2 (mild, 21%–40%), 3 (moderate, 41%–60%), 4 (severe, 61%–80%), 5 (very severe, >80%).

Cell isolation and flow cytometry

To isolate cells from inflamed tissues, lung tissues were cut into four pieces and gently stirred in flasks with solution (PBS containing 25 ml 10 mM EDTA, 3% FBS [HyClone Laboratories, Logan, UT, USA], 20mM HEPES and 1mM sodium pyruvate) for 30 min at 37°C. The segments were washed three times with PBS and digested with 5 ml RPMI 1640 containing 1 mg/ml of type V collagenase (Sigma-Aldrich, St. Louis, MO, USA) for 45 min at 37°C. Finally, the soup containing ear total cell was centrifuged and cultured in T cell media. For the surface marker staining, cells were washed with ice-cold PBS, re-suspended in 100 μl of PBS and stained with anti-CD3-BUV395, anti-CD45 (eBioscience, San Diego, CA, USA), anti-CD19-PE/Cy7 (BioLegend, San Diego, CA, USA), anti-CD4-FITC, anti-CD8-Percp5.5 (BioLegend). Dead cells were excluded using LiveDead Fixable Viability dye (Invitrogen, Waltham, MA, USA). Samples were acquired using ID7000 (Sony, Tokyo, Japan) and data were analyzed using FlowJo software (Tree Star, Ashland, OR, USA).

RNA sequencing (RNA-seq) and bioinformatic analyses

The lungs and spleens isolated from at 0, 1, 2, 5, 7 dpi of 1×10^5 PFU virus infected mice and at 0, 1, 2, 5, 7, 10, 14 dpi of 1×10^2 PFU virus infected mice were stored at −80°C in RNAlater solution. Tissues were moved to 1× PBS to remove residual RNAlater solution. Homogenization of tissues and total RNA extraction was conducted using a RNeasy plus mini kit (Qiagen, Valencia, CA, USA). Total RNA concentration was calculated by Quant-IT RiboGreen (#R11490; Invitrogen). To assess the integrity of the total RNA, samples are run on the TapeStation RNA screentape (#5067-5576; Agilent Technologies, Santa Clara, CA, USA). Only high-quality RNA preparations, with RIN greater than 7.0, were used for RNA library construction.

A library was independently prepared with 0.5 ug of total RNA for each sample by Illumina Stranded Total RNA Library Prep with Ribo-Zero Plus (#20040529; Illumina, Inc., San Diego, CA, USA). The first step in the workflow involves removing the rRNA in the total RNA. Following this step, the remaining mRNA is fragmented into small pieces using divalent cations under elevated temperature. The cleaved RNA fragments are copied into first strand cDNA using SuperScript II reverse transcriptase (#18064014; Invitrogen) and random primers. This is followed by second strand cDNA synthesis using DNA Polymerase I, RNase H and dUTP. These cDNA fragments then go through an end repair process, the addition of a single 'A' base, and then ligation of the adapters. The products are then purified and enriched with PCR to create the final cDNA library. The libraries were quantified using KAPA Library Quantification kits for Illumina Sequencing platforms according to the qPCR Quantification Protocol Guide (#KK4854; Kapa Biosystems, Wilmington, MA, USA) and qualified using the TapeStation D1000 ScreenTape (#5067-5582; Agilent Technologies). Indexed libraries were then submitted to an Illumina NovaSeq (Illumina, Inc.), and the paired-end (2×10^1 bp) sequencing was performed by the Macrogen Incorporated.

CLC Genomics Workbench 9.5.3 software (Qiagen GmbH, Hilden, Germany) was used to map the reads to the mouse genome (mm10, build name GRCm38) (**Supplementary Tables 1** and **2**) and SARS-CoV-2 viral genome (GenBank: MN985325.1) and generate gene expression values in the normalized form of transcripts per kilobase million. After checking

quality of samples, 23 (lungs) and 22 (spleen) samples at 0 (n=4; n=5), 1 (n=5; n=5), 2 (n=5; n=4), 5 (n=5; n=4), 7 dpi (n=4; n=4) were used for analysis in 1×10^5 PFU. For 1×10^2 PFU, total 28 (lungs) and 29 (spleen) samples at 0 (n=4; n=5), 1 (n=5; n=5), 2 (n=4; n=5), 5 (n=4; n=4), 7 (n=4; n=3), 10 (n=3; n=3), 14 dpi (n=4; n=4) were used. All differentially expressed genes (DEGs) were chosen based on the Benjamini–Hochberg false discovery rate (FDR)-adjusted p-value (i.e., q value <0.01) and two-fold differences by performing a statistical ANOVA of multiple groups. For Volcano and MA plots, a 2-group comparison analysis between the infected and non-infected control groups was performed using R package DESeq2, assuming negative binomial distribution. In MA plots, differentially expressing genes were chosen based on Benjamini–Hochberg FDR-adjusted p-value (i.e., q value <0.05). RStudio v3.6.3, which includes hierarchical clustering and principal components analysis, was used to analyze RNA-seq data. Gene Ontology (GO) enrichment analysis was performed using the R package clusterProfiler4 (15). Statistical significance was set at $p<0.05$. Immune cell deconvolution was performed using the R package immunedeconv (16).

Statistical analysis

Statistical significance was calculated using PRISM v9.0 software (GraphPad Software, San Diego, CA, USA). Error bars display SEM and significance was calculated using 2-way ANOVA with Bonferroni's multiple comparisons test.

RESULTS

Viral loads of SARS-CoV-2 influence mortality rates, and even low-dose infection induces pulmonary fibrosis

To determine the clinical characteristics of SARS-CoV-2 infection, we examined body weight loss and body temperature up to 14 dpi of the virus challenge. Compared with that in the negative control and at 0 dpi, the 1×10^2 PFU-infected mice exhibited a mild decrease in body temperature at 5–7 dpi and a decrease in body weight of approximately 20% at 5–8 dpi. Both clinical parameters steadily improved from 8 dpi to 14 dpi. In the 1×10^5 PFU-infected mice, however, severe clinical symptoms were observed; body temperature decreased dramatically to approximately 26.8°C at 4 dpi, and body weight was reduced by 25% (**Fig. 1A and B**). The survival rate varied with the infected viral dose; 50% of the 1×10^2 PFU-infected mice survived up to 14 dpi, whereas 83% of the 1×10^5 PFU-infected mice died at 7 dpi, and all died at 8 dpi (**Fig. 1C**). There were significant differences in the viral titers in the lungs at 2 dpi, reflecting different viral loads, but not at 7 dpi (**Fig. 1D**).

Then, we analyzed pulmonary pathology resulting SARS-CoV-2 infection. At 2 dpi, both 1×10^2 and 1×10^5 PFU-SARS-CoV-2-infected mice exhibited mild lesions (**Fig. 2A and B**). Inflammation due to the infiltration of immune cells, edema, and the capillary dilatation were the primary pathologies behind the lesions observed. The severity of the lesions and the pathology score were higher at 7 dpi than at 2 dpi (**Fig. 2C and D**). Even 1×10^2 PFU-infected mice exhibited fibrotic lesions at 7 dpi (**Fig. 2A and C**), despite an improvement in body temperature and body weight change after 8 dpi.

SARS-CoV-2 viral loads induce temporally different but transcriptionally similar changes in the lungs

We performed RNA-seq of SARS-CoV-2-infected lungs and spleens to examine the effects of viral concentration on the host response. Evaluation of data quality confirmed relatively

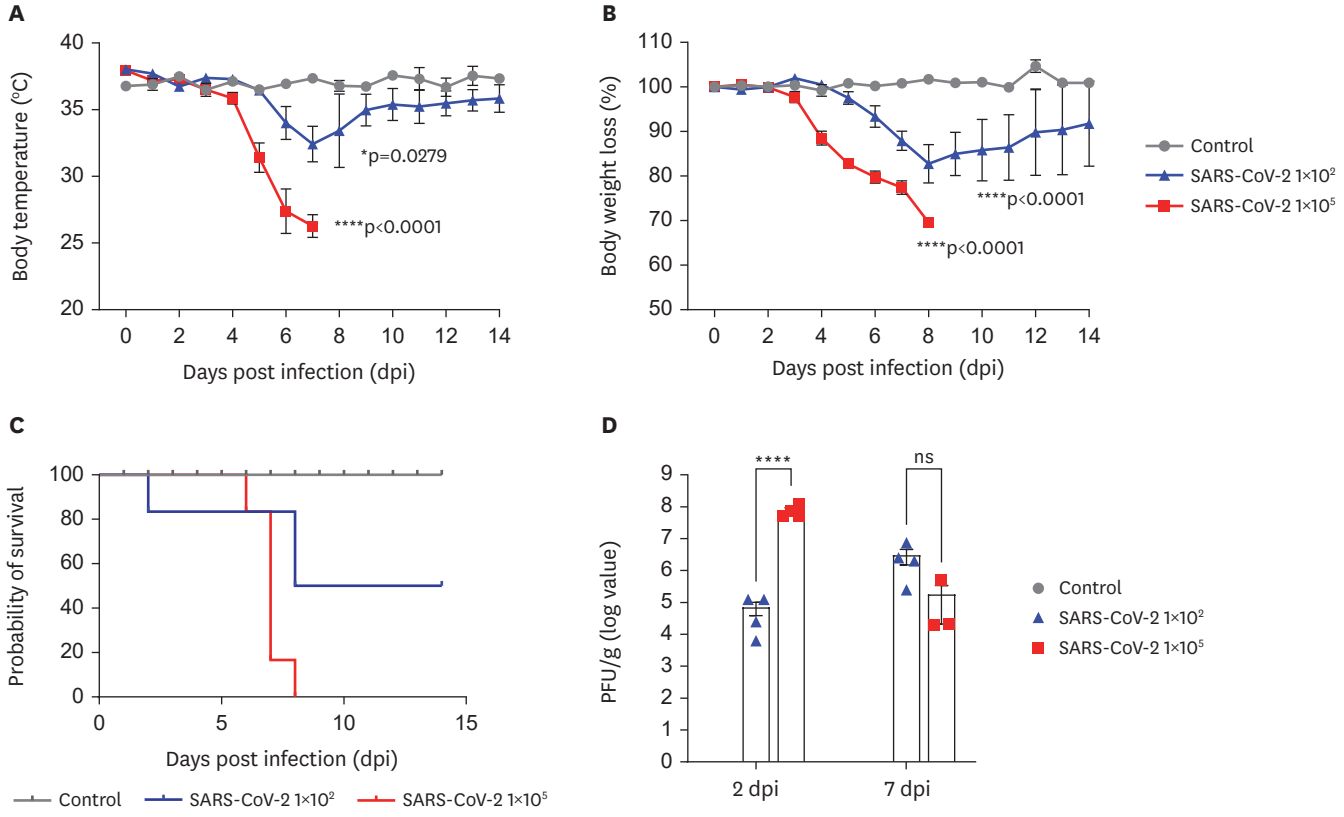

Figure 1. SARS-CoV-2 viral loads influence mortalities.
(A, B) Body temperature (A) and body weight (B) of PBS-infected control K18-hACE2 mice (n=6), 1×10^2 PFU-infected mice (n=8), and 1×10^5 PFU-infected mice (n=8). (C) Survival rate after infection with SARS-CoV-2. (D) Virus titer was measured at 2 and 7 dpi. Error bars are SEM and significance was calculated using 2-way ANOVA with Bonferroni's multiple comparison test.
*p<0.05; ****p<0.0001.

uniform transcriptome among samples (**Supplementary Fig. 1**). When the data were combined in a single PCA plot, the samples were segregated according to the organ, as determined by the principal component 1 (**Supplementary Fig. 2**). Principal component analysis plots demonstrated that transcriptomes of 1×10^5 PFU-infected mice's lungs and spleens were temporally distinct (**Supplementary Fig. 1**). The lung transcriptome profile of mice infected with 1×10^2 PFU showed that samples at 5, 7, and 10 dpi were projected away from early infection samples, whereas samples at 14 dpi were positioned adjacent to samples taken at 0 dpi (**Supplementary Fig. 1**), suggesting that the transcriptome of surviving mice returned to a non-infected state. The spleen samples from the 1×10^2 PFU-infected mice lacked a temporally distinct transcription profile and were not discretely divided into groups (**Supplementary Fig. 1**). To more precisely assess the extent of infection, we mapped the RNA-seq reads to the SARS-CoV-2 genome (**Supplementary Fig. 3**). In the lungs, the aligned portion of reads culminated at 2 dpi at 1×10^5 PFU and 7 dpi at 1×10^2 PFU, respectively. At the peak time point, the mean percentage of mapped reads of 1×10^5 PFU-infected lungs to the SARS-CoV-2 genome was approximately 15 times greater than that of 1×10^2 PFU SARS-CoV-2-infected lungs (**Supplementary Fig. 3**). The spleen samples at 1×10^5 PFU showed a progressive increase in the aligned portion from 2 to 7 dpi, although it was significantly lower than that in the lungs where nearly 40% of counts were aligned at 2 dpi at 1×10^5 PFU (**Supplementary Fig. 3**). Compared to that of 1×10^5 PFU-infected spleen samples, the aligned percentage of 1×10^2 PFU-infected spleen samples was barely detectable (**Supplementary Fig. 3**).

https://doi.org/10.4110/in.2024.24.e7

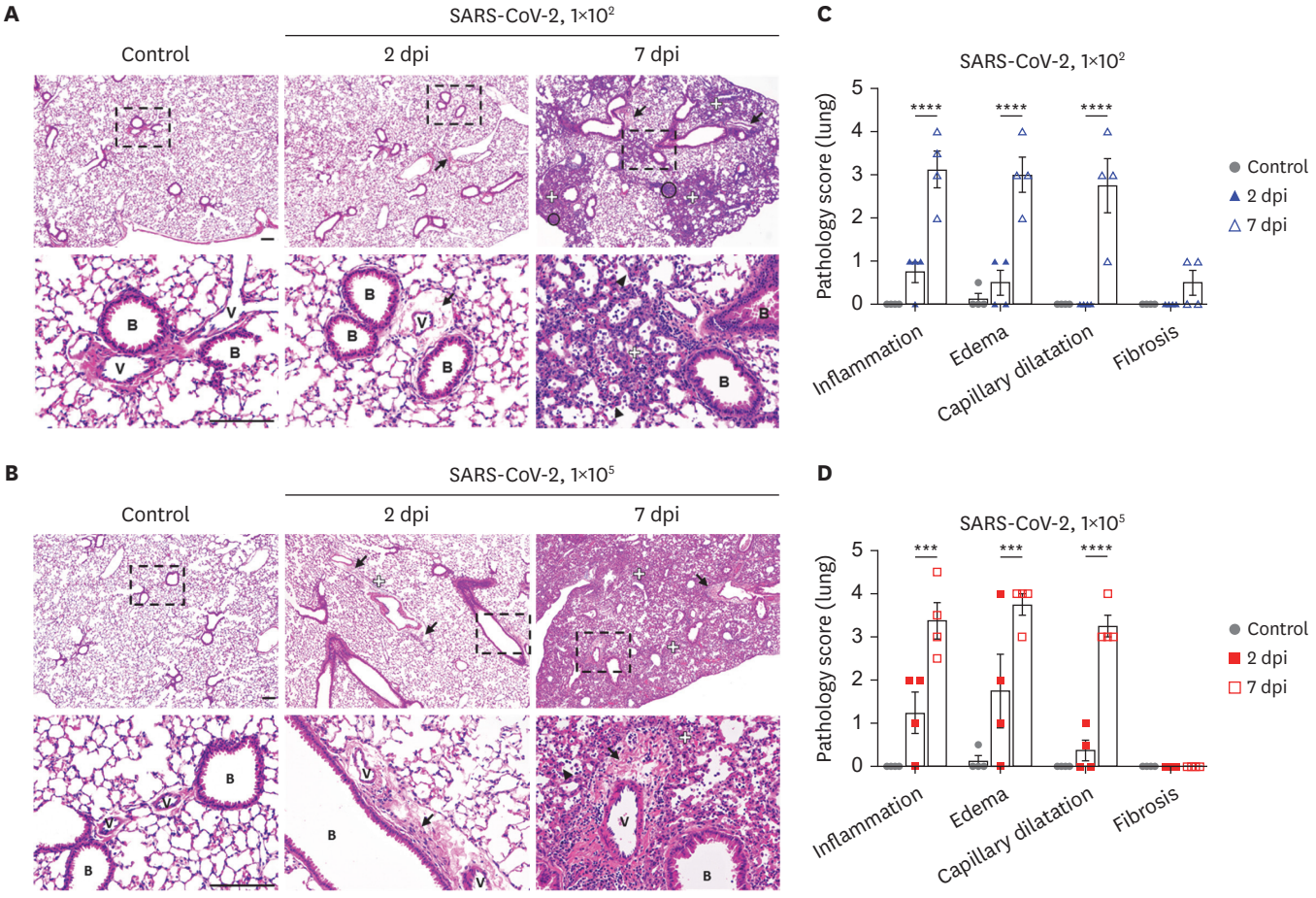

Figure 2. A lower dose of SARS-CoV-2 infection induces pulmonary fibrosis.
(A, B) H&E staining of lung sections in control, 1×10^2 PFU-, and 1×10^5 PFU-infected mice. Lungs infected with SARS-CoV-2 exhibit inflammation (white +), vascular edema (arrow), capillary dilatation (arrowhead), and pulmonary fibrosis (open circled). The letters 'B' and 'V' represent the bronchiole and vessel, respectively (scale bars, 100 μm). (C, D) Pathological score. Error bars are SEM and significance was calculated using 2-way ANOVA with Bonferroni's multiple comparison test. ***p<0.001; ****p<0.0001.

DEGs relative to non-infected controls were identified at different time points. MA plots revealed that the number of DEGs increased over time after infection with a 1×10^5 PFU viral load (**Supplementary Fig. 4**), while it remained relatively constant regardless of the time course at 1×10^2 PFU in both organs; however, fewer genes were differentially expressed in spleens (**Supplementary Fig. 4**).

Multiple comparisons identified 1,348 and 1,094 DEGs in the lungs of mice infected with 1×10^5 PFU- and 1×10^2 PFU, respectively. At each dose, hierarchical clustering identified three and four patterns respectively, in the lungs (**Supplementary Figs. 5** and **6**). The GO analysis of DEGs with particular expression patterns revealed that these genes are implicated in the same biological processes in the infected lungs, irrespective of the viral doses (**Supplementary Figs. 5** and **6**, **Supplementary Table 3**). These biological processes were immunoglobulin production, chromosome segregation, and response to the virus (**Supplementary Figs. 5** and **6**). Several distinct pathways were also identified, but there were no significant distinctions between the representative enriched terms as a whole (**Supplementary Figs. 5**, **6**, and **Supplementary Table 3**). However, DEGs within the same GO term displayed distinct temporal expression patterns in the lungs infected with 1×10^5 PFU- and 1×10^2 PFU (**Fig. 3A and B**). In the lungs

of mice infected with 1×10^5 PFU, the genes associated with the response to the virus were found to be significantly upregulated at 2 dpi (**Fig. 3A**). However, when the mice were infected with 1 × 10^2 PFU, the activation of these genes was delayed and increased after 5 dpi (**Fig. 3B**). By 14 dpi, the expression of these genes in the lungs of mice infected with 1×10^2 PFU reverted to the levels observed in non-infected control animals (**Fig. 3B**). The same expression pattern was observed in type I and II interferon signaling as well as cytokine-mediated signaling, which were found to be stimulated by SARS-CoV-2 infection (12) (**Supplementary Fig. 7**). Immunoglobulin production, primarily the immunoglobulin kappa variable cluster, decreased in the lungs at both doses as viral infection progressed (**Fig. 3A and B**). Furthermore, genes associated with chromosome segregation were increased from 5 dpi at both doses (**Fig. 3A and B**). Meanwhile, in the lungs of 1 × 10^2 PFU-infected mice, genes associated with muscle contraction decreased until 5 dpi and subsequently increased (**Fig. 3B** and **Supplementary Fig. 6E**).

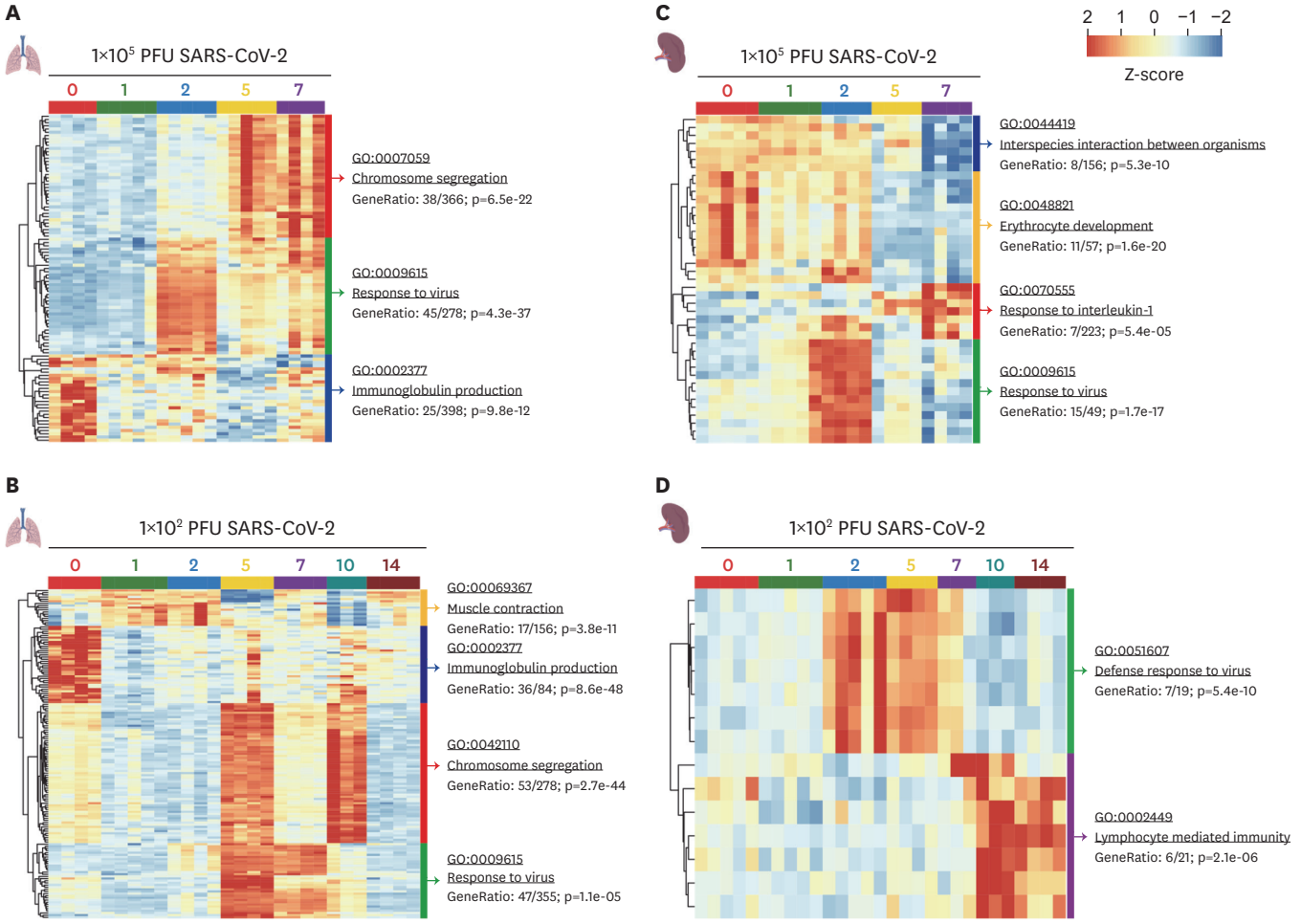

Figure 3. Viral loads of SARS-CoV-2 induce temporally distinct but equivalent transcriptional changes in the lungs, while only 1×10^5 PFU SARS-CoV-2 induced obvious immune response in spleens.
(A) Heatmap for 108 DEGs with 1×10^5 PFU-infected lungs (red: 0 dpi, green: 1 dpi, blue: 2 dpi, yellow: 5 dpi, purple: 7 dpi). (B) Heatmap for 153 DEGs with 1×10^2 PFU-infected lungs (red: 0 dpi, green: 1 dpi, blue: 2 dpi, yellow: 5 dpi, purple: 7 dpi, cyan: 10 dpi, dark red: 14 dpi). (C) Heatmap for 41 DEGs with 1×10^5 PFU-infected spleens (red: 0 dpi, green: 1 dpi, blue: 2 dpi, yellow: 5 dpi, purple: 7 dpi). (D) Heatmap for 13 DEGs with 1×10^2 PFU-infected spleens (red: 0 dpi, green: 1 dpi, blue: 2 dpi, yellow: 5 dpi, purple: 7 dpi, cyan: 10 dpi, dark red: 14 dpi).
The enriched GO terms of the biological process are displayed on the right side of heatmaps.

https://doi.org/10.4110/in.2024.24.e7

Immunological response in the spleens is obvious at 1×10^5 PFU but not at 1 × 10^2 PFU- SARS-CoV-2 infection

In the spleens of 1×10^5 PFU- and 1×10^2 PFU-infected mice, analysis of variance identified 700 and 49 DEGs (**Supplementary Figs. 8** and **9**). Hierarchical clustering analysis revealed that genes were expressed in four distinctive patterns in the 1×10^5 PFU-infected mice spleens (**Supplementary Fig. 8**). At 1×10^2 PFU, two patterns were observed (**Supplementary Fig. 9**) and DEGs were changed little compared to 1×10^5 PFU. GO terms representing immune-related processes were significantly enriched at 1×10^5 PFU compared to 1×10^2 PFU (**Supplementary Fig. 8**, **Supplementary Table 4**). At 1×10^2 PFU, however, the majority of DEGs were associated with innate or adaptive immune responses, such as negative regulation of viral genome replication and lymphocyte-mediated immunity (**Supplementary Fig. 9**, **Supplementary Table 4**).

When we selected representative GO terms enriched in DEGs for each pattern, the defense response to virus was observed in the spleens at both dosages (**Fig. 3C and D**). Specifically, interferon-stimulated genes, such as the *Oas* gene family, *Ifit1*, *Ifit3b*, and *Mx2,* which participate in the immediate defense response upon viral intrusion, were highly expressed in the spleens during the early phase of infection at both doses (**Fig. 3C and D**). In particular, the expression of these genes peaked at 2 dpi in the spleens of 1×10^5 PFU-infected mice, just as it did in the lungs (**Fig. 3A and C**). Chemokine-mediated immunity genes exhibited similar expression patterns (**Supplementary Fig. 10**). Genes involved in interspecies interaction between organisms showed an abrupt decrease at 7 dpi in 1×10^5 PFU-infected spleens (**Fig. 3C**). Genes related to erythrocyte development pathway were decreased from 5 to 7 dpi in 1×10^5 PFU-infected spleens (**Fig. 3C**). Genes associated with response to IL-1 were dramatically upregulated during the late phase of infection at the 1×10^5 PFU dose (**Fig. 3C**). At 1×10^2 PFU, the number of DEGs was low, but, lymphocyte-mediated immunity, notably orchestrated by B cells, was enhanced from 10 dpi (**Fig. 3D**). Particularly, neutralizing Abs, such as *Ighv1-3*, *Ighe*, *Ighv2-6*, and *Ighv9-2*, were increased from 10 dpi (**Fig. 3D**).

SARS-CoV-2 concentrations determine gene expression levels and temporal changes associated with immune response

We conducted a gene set variation analysis (GSVA) using GO terms associated with immune response (**Fig. 3**) to compare the temporal changes in gene expression based on virus concentration (**Fig. 4A**). At 1 × 10^5 PFU, the majority of genes involved in the response to the virus exhibited the highest expression at 2 dpi in the lungs, followed by a slight decrease until 7 dpi (**Fig. 4A**). *Cxcl10* and *Il6* expression peaked at 2 dpi in the lungs of mice infected with 1×10^5 PFU (**Fig. 4B**), whereas *Cxcl10* and *Il6* exhibited delayed expression at 5 dpi at 1×10^2 PFU, but their maximal expression levels were lower than those at 1×10^5 PFU (**Fig. 4B**). Interestingly, at 14 dpi, *Cxcl10* and *Il6* expression seemed to gradually return to basal levels seen at 0 dpi (**Fig. 4B**), indicating normalization of gene expression in the lungs of mice that survived infection with 1×10^2 PFU.

Similar to what was observed in the lungs, genes activated against viral intrusion were highly expressed in the spleens during the early phase of infection, and their expression substantially decreased at 7 dpi (**Fig. 4C**). In the spleens of mice infected with 1×10^5 PFU, *Cxcl10* and *Il6* expression peaked at 2 dpi and returned to almost basal levels by 7 dpi even though mice died. At 1×10^2 PFU, *Cxcl10* and *Il6* expression were increased at 2 dpi; however, the expression level was significantly lower than that at 1×10^5 PFU, and similar expression levels were maintained until 5 dpi (**Fig. 4D**). *Cxcl10* and *Il6* expression decreased consistently

https://doi.org/10.4110/in.2024.24.e7

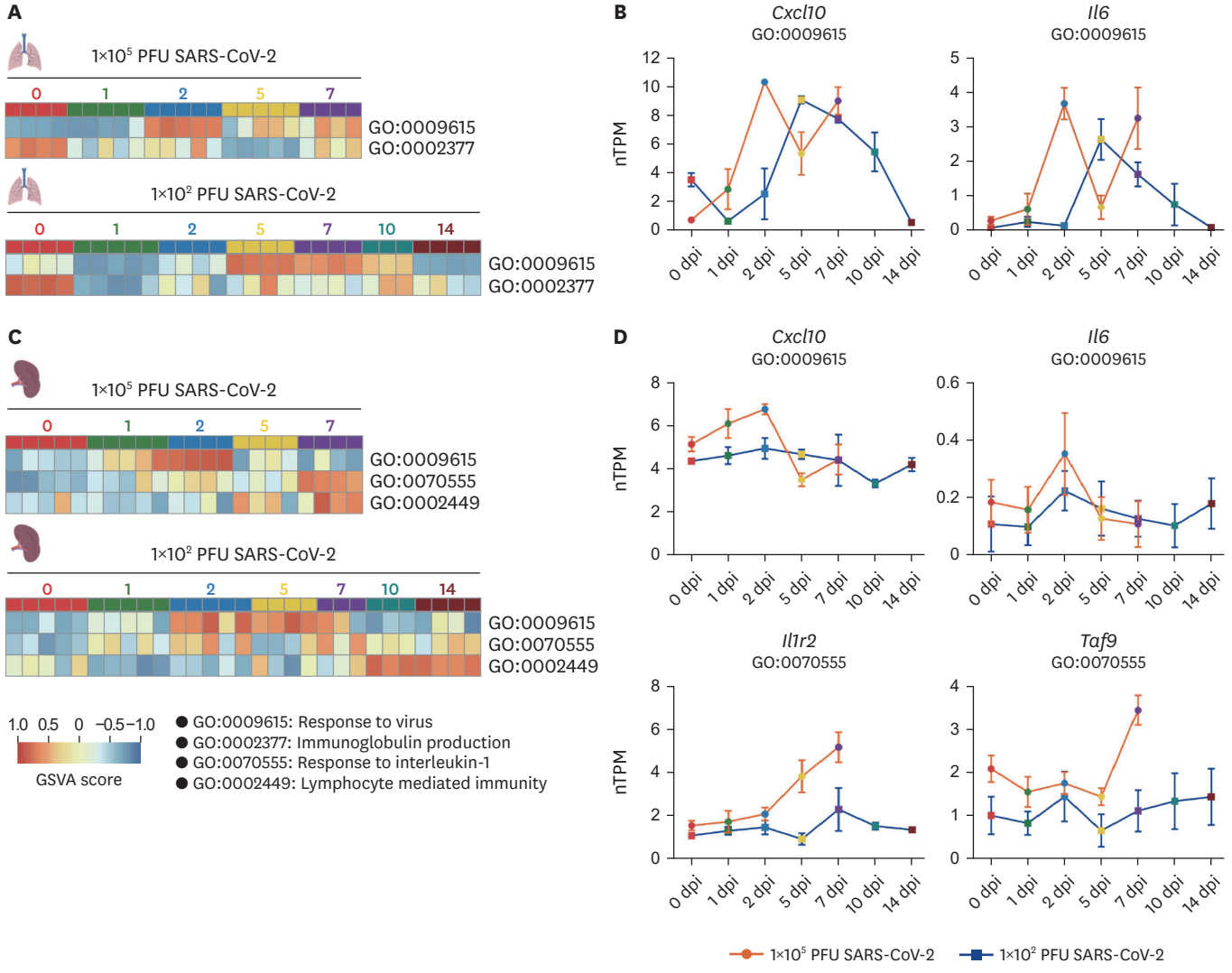

Figure 4. SARS-CoV-2 dosage determines gene expression levels and temporal changes in immune response-related genes.
(A) Heatmaps of the GSVA results for response to virus (GO: 0009615) and immunoglobulin production (GO: 0002377) in lungs infected with 1×10^5 PFU or 1×10^2 PFU. (B, D) Graphs illustrating the temporal changes in expression levels caused by SARS-CoV-2 infection for representative genes (orange: 1×10^5 PFU, blue: 1×10^2 PFU). (C) Heatmaps for GSVA results for response to virus (GO: 0009615), response to IL-1 (GO: 0070555), and lymphocyte mediated immunity (GO: 0002449) in spleens.

after 5 dpi and finally returned to basal levels at 14 dpi (**Fig. 4D**). In contrast, at 7 dpi, genes related to response to IL-1 were markedly upregulated in the spleens of mice infected with 1×10^5 PFU (**Figs. 3C** and **4C**). For example, *Il1r2* and *Taf9* exhibited no variation in expression during the early period, but reached their highest level at 7 dpi at 1×10^5 PFU. However, their expression remained nearly constant at 1×10^2 PFU (**Fig. 4D**). The recovery of expression of immunomodulatory genes such as *Oas*, *Ifit*, and *Mx* at 1×10^2 PFU may have allowed for further survival of SARS-CoV-2-infected K18-hACE2 transgenic mice, whereas the virus at 1×10^5 PFU virus prevented adequate recovery of both organs (17-19).

Specific immune effector cell populations are differentially affected by viral loads in the lungs and spleens

To further characterize the immune response induced by varying concentrations of SARS-CoV-2, we used an *in silico* deconvolution tool that infers cell-type fractions from bulk RNA-seq data (16). The results of deconvolution revealed the differences in the relative amounts

https://doi.org/10.4110/in.2024.24.e7

of adaptive immune effectors (**Supplementary Figs. 11** and **12**). In the lungs, the number of transcripts associated with CD8+ T cells increased at 5 and 10 dpi in the 1×10^2 PFU-infected mice compared to non-infected controls, but not in the 1×10^5 PFU-infected mice at any time point (**Supplementary Fig. 11**). T cell activation was one of the GO terms for genes that displayed pattern B in the lungs of 1×10^2 PFU-infected mice (**Supplementary Fig. 6B**). Furthermore, our immunohistochemical analysis revealed a progressive and significant increase in CD8+ T cells in the lungs of mice infected with 1×10^2 PFU, as compared to mice infected with 1×10^5 PFU (**Fig. 5A**). To confirm this, we conducted flow cytometry experiments to determine the T cell fraction in 1×10^5 PFU-and 1×10^2 PFU-infected lungs (**Fig. 5B and C**,

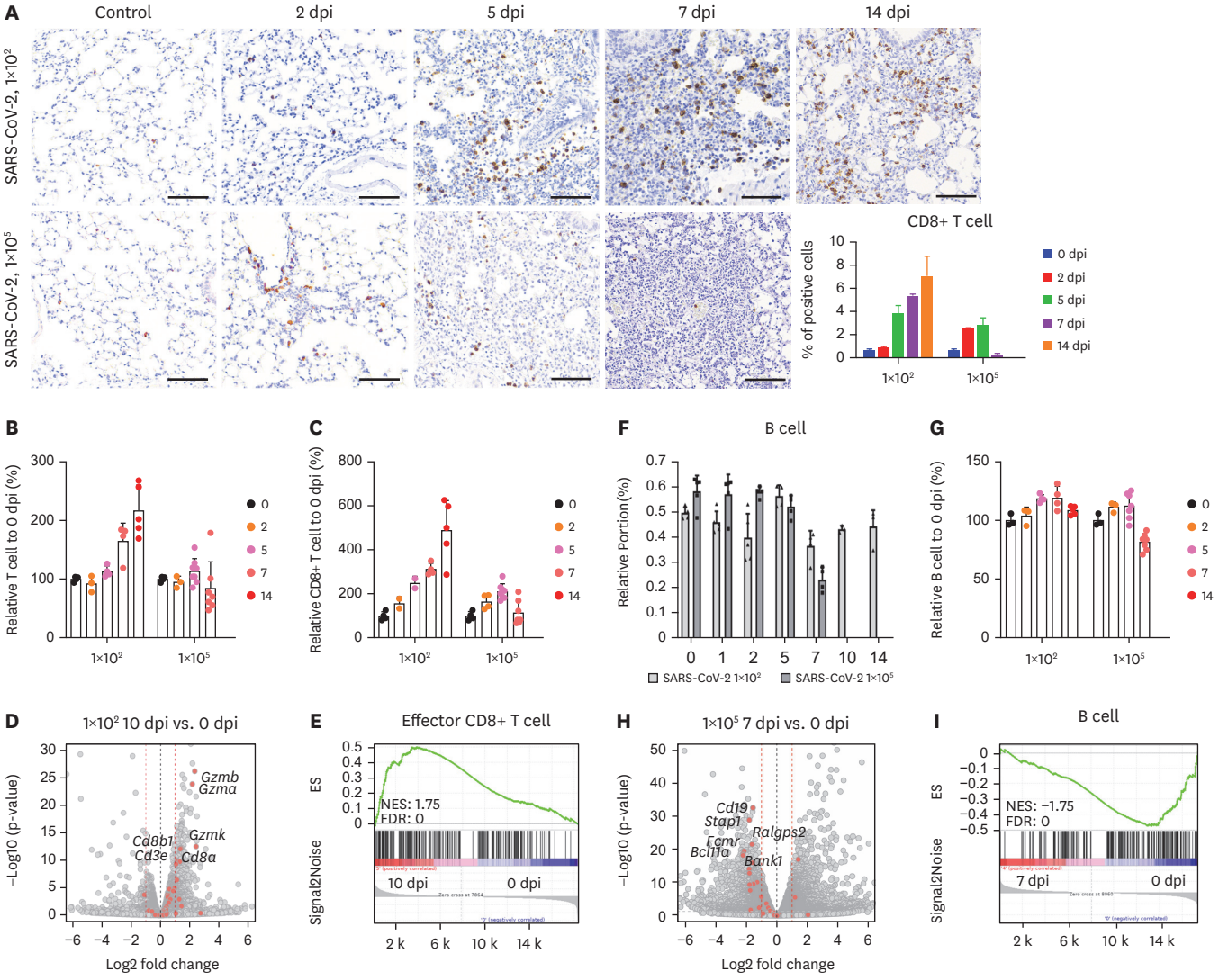

Figure 5. Changes in CD8+ T cells and B cells in the lungs and spleens of SARS-CoV-2 infected mice.
(A) Immunohistochemistry for CD8+ T cells during the progression of infection. The graph depicts the number of CD8+ cells relative to total number of cells at 40× high power field (scale bars, 50 μm). (B, C) Flow cytometric analysis of total T cells (B) and CD8+ T cells (C) in SARS-CoV-2-infected lungs at 2, 5, 7, or 14 dpi with SARS-CoV-2 (left: 1×10^2 PFU, right: 1×10^5 PFU). A 0 dpi indicates naïve mice. Bars represent the relative proportion of T cells in each dpi relative to naïve mice (at least 2 independent experiments per group). (D) Volcano plots comparing total genes from lung samples collected at 10 dpi relative to 0 dpi at 1×10^2 PFU. Red indicates 28 genes that were related to T cell identification and profiling in the previous studies (21,22). The 6 most significant genes are labeled. (E) Gene set enrichment analysis for genes related to cytolytic CD8+ effector T cells (22). (F) Immune deconvolution results identifying B cell composition in the spleens. Bars represent mean ± SEM. (G) Flow cytometric analysis of B cells in SARS-CoV-2-infected spleens at 2, 5, 7, or 14 dpi with SARS-CoV-2 (left: 1×10^2 PFU, right: 1×10^5 PFU). A 0 dpi indicates naïve mice. Bars represent the relative proportion of B cells in each dpi relative to naïve mice (at least 2 independent experiments per group). (H) Volcano plots comparing total genes from spleen samples collected at 7 dpi relative to 0 dpi at 1×10^5 PFU. Red represents the 32 B cell markers utilized in the immune deconvolution analysis. The 6 most significant markers are labeled. (I) Gene set enrichment analysis for genes related to adaptive B2 lymphocytes (23).

https://doi.org/10.4110/in.2024.24.e7

Supplementary Fig. 13). The results revealed that the total T cell proportion increased continuously from 5 to 14 dpi at 1×10^2 PFU, whereas no significant difference was observed in the total T cell composition of 1×10^5 PFU-infected lungs when compared to 0 dpi (**Fig. 5B**, **Supplementary Fig. 13A**). It also demonstrated that the proportion of CD8+ T cell portion in 1×10^2 PFU-infected lungs increased up to 2-fold from 2 to 14 dpi (**Fig. 5C**). In contrast, CD4+ T cell proportion in 1×10^2 PFU-infected lungs did not increase until 14 dpi (**Supplementary Fig. 13B**). After we confirmed the consistency between deconvolution result and flow cytometry data, we attempted to examine the specific expression of much more diverse marker genes associated with T cell in the 10 dpi of 1×10^2 PFU-infected lungs. We selected 28 marker genes related to T cell identification and profiling (20,21) and labeled 6 highly significant markers among them on volcano plots (**Fig. 5D**). Expression of granzyme B, which is detected at significantly higher frequencies in SARS-CoV-2–specific T cells of convalescent donors (21), was significantly upregulated at 10 dpi in the 1×10^2 PFU-infected mice lungs (**Fig. 5D**). The subsequent gene set enrichment analysis revealed that genes related to cytolytic effector CD8+ T cells (22) were highly enriched by SARS-CoV-2 infection at 10 dpi in the 1×10^2 PFU-infected mice lungs (**Fig. 5E**). In conclusion, the number of CD8+ T cell in the lungs increased continuously from 2 dpi by 1×10^2 PFU, but not by 1×10^5 PFU SARS-CoV-2.

Changes in the proportion of B cells were prominent among immune effectors in the spleens, whereas other immune cell types exhibited only minor variations (**Fig. 5F**, **Supplementary Fig. 12**). Specifically, the proportion of transcripts associated with B cells dropped precipitously at 7 dpi in the spleens of 1×10^5 PFU-infected mice (**Fig. 5F**). Throughout the time course, the number of transcripts associated with B cells in the 1×10^2 PFU-infected mice spleens did not differ significantly from that 1×10^5 PFU-infected mice spleens (**Fig. 5F**). Subsequent experimental quantification of B cell composition via flow cytometry corroborated deconvolution analysis results demonstrating a decrease in B cell fraction at 7 dpi in 1×10^5 PFU (**Fig. 5G**, **Supplementary Fig. 14**). Volcano plots confirmed that the expression of B cell marker genes in the spleens of 1×10^5 PFU-infected mice was lower at 7 dpi compared to non-infected controls (**Fig. 5H**). In addition, genes associated with adaptive B2 lymphocytes (23) demonstrated a significant negative enrichment in the 7 dpi spleen samples at 1×10^5 PFU (**Fig. 5I**). CD8+ T cells and B cells each responded differentially to various viral concentrations in the lungs and spleens.

Pulmonary fibrosis occurs as a sequela of low-dose SARS-CoV-2

Histopathological data demonstrated that fibrosis progressed in the lungs of mice infected with 1×10^2 PFU SARS-CoV-2 at 7 dpi (**Fig. 2A and C**). With 1×10^5 PFU, however, no pulmonary fibrosis was observed (**Fig. 2B and D**). Although clinical and transcriptome results indicated that the intense immune response exerted by infiltrating immune cells was predominant at both dosages, pulmonary fibrosis was only observed at the lower dose. For this reason, we further investigated the transcriptional changes in genes associated with pulmonary fibrosis over time. The expression of some fibrosis-associated genes reached its peak at 5 dpi in the lungs of mice infected with a viral dose of 1×10^2 PFU (**Fig. 6A**). At 7 dpi, most genes exhibited a moderate level of expression in the lungs. This expression of some fibrosis-related genes, such as *Ccl2*, *Ccl3*, *Ccl4*, *Mt2*, *Plau* and *Timp1*, remained consistent until 10 dpi after exposure to 1×10^2 PFU (**Fig. 6A**). In contrast, about half of genes were increased till 7 dpi at 1×10^5 PFU (**Fig. 6A**).

We also examined the enrichment of lung fibrosis gene set from the Molecular Signatures Database. At 1×10^5 PFU, fibrosis-related genes were positively enriched at all time points (**Fig. 6B**). At 1×10^2 PFU, these genes began to be positively enriched from 5 to 10 dpi, and their expression decreased at 14 dpi (**Fig. 6C**). While fibrosis-related genes were found to be

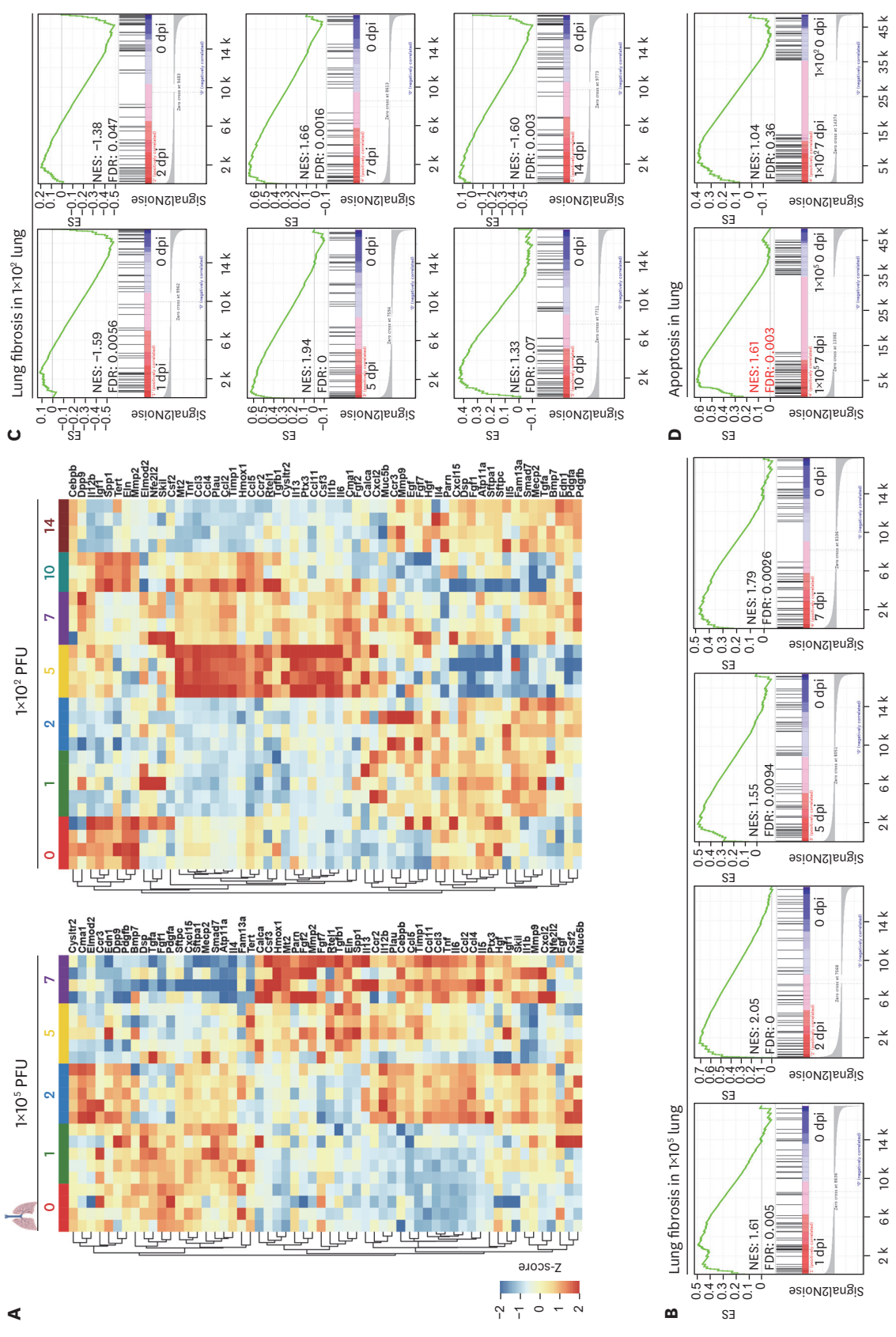

Figure 6. Genes associated with pulmonary fibrosis are upregulated by SARS-CoV-2 infection.
(A) Heatmaps for genes related to pulmonary fibrosis in the lungs (top: 1×10^5 PFU, bottom: 1×10^2 PFU). (B, C) Gene set enrichment analysis for genes associated with lung fibrosis using C2 gene sets from molecular signatures database (MsigDB) at 1×10^5 PFU (B) and at 1×10^2 PFU (C). (D) Gene set enrichment analysis of for genes associated with apoptosis using C2 gene sets from MsigDB (left: 7 dpi versus 0 dpi 1×10^5 PFU, right: 7 dpi versus 0 dpi 1×10^2 PFU).

https://doi.org/10.4110/in.2024.24.e7

elevated at both 1×10^5 PFU and 1×10^2 PFU, the enrichment of apoptosis was only significant at 1×10^5 PFU (**Fig. 6D**). These results suggest that pulmonary fibrosis may be a comorbidity or complication associated with SARS-CoV-2 long-term infection.

DISCUSSION

In this study, we conducted a transcriptome analysis and flow cytometry to obtain insight into the dose-dependent host response to SARS-CoV-2 in lungs and spleens of K18-hACE2 mice. The results demonstrated that CD8+ T cells were increased in 1×10^2 PFU-infected lungs, whereas B cells were decreased in 1×10^5 PFU-infected spleens. In 1×10^2 PFU-infected lungs, pulmonary fibrosis and the upregulation of fibrotic genes were also observed.

Prior research involving the inoculation of ferrets with high (5×10^6 PFU), medium (5×10^4 PFU), and low (5×10^2 PFU) titers of SARS-CoV-2 revealed that the high- and medium-dose groups exhibited high pathology scores (10). In addition, mild multifocal bronchopneumonia was observed, particularly at 3 and 5 dpi, corroborating our results (10). In contrast to our findings, viral RNA was not detectable in the lungs of high- and medium-dose-infected ferrets (10). Our observation of pulmonary fibrosis at 1×10^2 PFU was the most significant difference between our histology data and the previous study report (10). In addition, no signs of pulmonary fibrosis were observed in the histopathology of animals infected with UV-inactivated SARS-CoV or SARS-CoV-2 in previous studies (24,25). Although fibrotic genes were increased in the lungs with a viral load of 1×10^5 PFU, it appeared that the initiation of apoptosis may have hindered the progression of pulmonary fibrosis at 7 dpi in mice infected with 1×10^5 SARS-CoV-2. Pulmonary fibrosis is a common complication in patients with COVID-19 (26) and developed in the post-discharge phase of more than one-third of the infected patients who survived severe COVID-19 pneumonia (27,28). Cytokine storms may have inflicted repetitive injuries on the alveolar epithelium. In addition to the massive cytokine secretion, an imbalance between proteases and their inhibitors may have contributed to the excessive accumulation of extracellular matrix during tissue reconstruction (29). The correlation between the severity of infection and pulmonary fibrosis is not fully understood. Nonetheless, our study on 1×10^2 PFU-infected mice demonstrating the occurrence of fibrosis suggests that persistent infection can leave permanent histological scars and further impede normal ventilatory function by decreasing the capacity for gas exchange.

Lung transcriptome profiles revealed that viral loads influenced the temporal variations. In particular, the expression of immunomodulatory mediators in the lungs of 1×10^2 PFU-infected mice was delayed by approximately 3 days. Prediction of immune effector types that infiltrate lungs provides insight into the mechanism that may help the host avoid lethality and manage survival at 1×10^2 PFU. After 2 dpi, CD8+ T cells increased in 1×10^2 PFU-infected lungs. Intriguingly, the enhanced regeneration of these effectors occurred 14 days after infection. This phenomenon is noteworthy because the recovery of immunocompetence following hematopoietic stress or injury is essential for effective pathogen responses (30).

1×10^5 PFU of SARS-CoV-2 induced diverse immune-related responses in the spleens. Notably, inflammation-related pathways were significantly upregulated during the late phase of infection in the spleens of mice infected with 1×10^5 PFU. Hyperinflammation may result from excessive stimulation of multiple inflammatory pathways. Despite the fact that the cascade of cytokine release eliminated the virus, tissue destruction and organ failure were inevitable.

In contrast, at a lower dose, temporal change appeared negligible, as indicated by the small number of DEGs. At 7 dpi, the proportion of B cells was significantly reduced in the spleens of 1×10^5 PFU-infected mice. Continued B cell depletion compromises the adaptive immune response and the ability to produce neutralizing Abs, thereby exacerbating the severity of persistent COVID-19 in patients (31). A deficient B cell immune segment in the late period is indicative of severe spleen destruction at lethal virus concentrations.

Despite the fact that this study determined the dose-dependent host response of SARS-CoV-2-infected lungs and spleens in K18-hACE2 mice, the mortality fate of each 1×10^2 PFU-infected animal could not be predicted. Since we did not track animal survival and sacrificed them at specific time points for experiments, it is challenging to predict which mice were destined to die or survive based on early infection-stage clinical and transcriptome data.

Combining the aforementioned observations, we deduced that the 1×10^5 PFU virus concentration may have triggered irreversible organ failure in the lungs and spleens, resulting in death. At 1×10^2 PFU, however, recovery of activated defense mechanisms in the lungs to basal expression levels could have helped the host avoid death. The effects of compositional shifts in adaptive immune cell types at specific infection time points may also be associated with increased survival. However, animals that survive long-term infections may experience complications, such as fibrosis, following recovery.

ACKNOWLEDGEMENTS

This study was supported by the National Research Foundation of Korea (NRF) funded by the Korean government (MSIT) (2020M3A9D5A01082439 and 2018R1A5A2025079 to H.Y.G., 2016M3A9D5A01952416 to K.T.N, and Bio & Medical Technology Development Program 2021M3H9A1038083 to K.T.N).

SUPPLEMENTARY MATERIALS

Supplementary Table 1
Reads statistics of RNA sequencing data

Supplementary Table 2
Reads statistics of RNA sequencing data

Supplementary Table 3
DEGs used in GO analysis in **Fig. 3A and B**

Supplementary Table 4
DEGs used in GO analysis in **Fig. 3C and D**

Supplementary Figure 1
Principal component analysis of RNA-seq data of the lungs and spleens of mice infected with SARS-CoV-2 by dose. Box plots (left) indicate that normalized transcripts of all samples are equally distributed. Normalized TPM of 48,440 genes were used for analyses.

Supplementary Figure 2
Principal component analysis of RNA-seq data of total samples.

Supplementary Figure 3
Proportion of sequence reads that map to the SARS-CoV-2 viral genome. (A-B) The bar plots show the percentage of reads mapped to SARS-CoV-2 virus genome (GenBank: MN985325.1). Percentage of mapped reads was calculated by dividing counted fragments with total fragments aligned to the respective reference genome. Red represents non-infected controls, while black indicates infected samples.

Supplementary Figure 4
Distribution of differentially expressing genes following the progression of infection. MA plots comparing the total genes in organs infected with 1×10^5 PFU- and 1×10^2 PFU. Yellow represents lung samples, while blue represents spleen samples. The transparent color indicates 1×10^2 PFU. Blue dots represent genes with the 5% FDR threshold. The number of blue dots is indicated.

Supplementary Figure 5
Transcriptional changes in the lungs of K18-hACE2 transgenic mice infected with 1×10^5 PFU SARS-CoV-2. (A) Heatmap for 1,348 DEGs. DEGs were classified into 3 expression patterns. The gene expression levels in the heatmap are z-score normalized TPM values. (B-D) GO analysis of DEGs. After analyzing the GO category representing biological process and removing redundant terms, the top 15 GO terms were listed. The color and size of each dot represent p-value and gene ratio (gene counts in specific term/total genes), respectively.

Supplementary Figure 6
Transcriptional changes in the lungs of K18-hACE2 transgenic mice infected with 1×10^2 PFU SARS-CoV-2. (A) Heatmap for 1,094 DEGs. DEGs were classified into 4 expression patterns. The gene expression levels in the heatmap are z-score normalized TPM values. (B-E) GO analysis of DEGs. After analyzing the GO category representing biological process and removing redundant terms, the top 15 GO terms were listed. The color and size of each dot represent p-value and gene ratio (gene counts in specific term/total genes), respectively.

Supplementary Figure 7
Transcriptional alterations of immune-related genes in lungs induced by SARS-CoV-2 infection. Heatmaps of significantly upregulated genes associated with cytokine-mediated signaling pathway, type I interferon, and cellular response to IFN-γ. The gene sets are from a prior study (12). Top: 1×10^5 PFU-infected lungs; Bottom: 1×10^2 PFU-infected lungs. Rows represent genes, while columns represent samples. The gene expression levels in the heatmaps are z-score normalized TPM values.

Supplementary Figure 8
Transcriptional changes in the spleen of K18-hACE2 transgenic mice infected with 1×10^5 PFU SARS-CoV-2. (A) Heatmap for 700 DEGs. DEGs were classified into 4 expression patterns. The gene expression levels in the heatmaps are z-score normalized TPM values. (B-E) GO analysis of DEGs. After analyzing the GO category representing biological process and removing redundant terms, the top 15 GO terms were listed. The color and size of each dot represent p-value and gene ratio (gene counts in specific term/total genes), respectively.

Supplementary Figure 9

Transcriptional changes in the spleen of K18-hACE2 transgenic mice infected with 1×10^2 PFU SARS-CoV-2. (A) Heatmap for 49 DEGs. DEGs were classified into 2 expression patterns. The gene expression levels in the heatmaps are z-score normalized TPM values. (B-C) GO enrichment analysis of DEGs. After analyzing the GO category representing biological process and removing redundant terms, the top 15 GO terms were listed. The color and size of each dot represent p-value and gene ratio (gene counts in specific term/total genes), respectively.

Supplementary Figure 10

Transcriptional alterations of immune-related genes in spleen induced by SARS-CoV-2-infection. Heatmaps of significantly upregulated genes associated with cytokine-mediated signaling pathway, type I interferon, and cellular response to IFN-γ. The gene sets are from a prior study (12). Top: 1×10^5 PFU-infected spleen; Bottom: 1×10^2 PFU-infected spleen. Rows represent genes, while columns represent samples. The gene expression levels in the heatmaps are z-score normalized TPM values.

Supplementary Figure 11

Transcriptome-based immune cell quantification in the lungs of SARS-CoV-2-infected K18-hACE2 transgenic mice. Immune deconvolution was done using the immunedeconv to identify immune cell composition in the 1×10^5 PFU- and 1×10^2 PFU-infected lungs. Bars represent mean ± SEM. Dark gray: 1×10^5 PFU-infected lungs, Light gray: 1×10^2 PFU-infected lungs.

Supplementary Figure 12

Transcriptome-based immune cell quantification in the spleen of SARS-CoV-2-infected K18-hACE2 transgenic mice. Immune deconvolution was done using the immunedeconv to identify immune cell composition in the 1×10^5 PFU- and 1×10^2 PFU-infected spleen. Bars represent mean ± SEM. Dark gray: 1×10^5 PFU-infected spleen, Light gray: 1×10^2 PFU-infected spleen.

Supplementary Figure 13

Flow cytometry of T cell fraction in SARS-CoV-2-infected lungs. (A) Histograms of T cell fraction in lungs. Representative flow cytometric plots and frequencies of T cells (CD3+TCRb+) in lung tissues at 0, 2, 5, 7, or 14 dpi from SARS-CoV-2-infected K18-hACE2 mice (upper: 1×10^2 PFU, lower: 1×10^5 PFU). At least 2 independent experiments per group. (B) Changes in CD4+ T cells in lungs during SAR2-CoV-2 infection. A 0 dpi indicates naïve mice.

Supplementary Figure 14

Flow cytometry of B cell fraction in SARS-CoV-2-infected spleens. Representative flow cytometric plots and frequencies of B cells (CD19+TCRb−) in spleen tissues at 0, 2, 5, 7, or 14 dpi from SARS-CoV-2-infected K18-hACE2 mice. At least 2 independent experiments per group.

REFERENCES

1. Zhu N, Zhang D, Wang W, Li X, Yang B, Song J, Zhao X, Huang B, Shi W, Lu R, et al. A novel coronavirus from patients with pneumonia in China, 2019. *N Engl J Med* 2020;382:727-733. PUBMED | CROSSREF
2. Cui J, Li F, Shi ZL. Origin and evolution of pathogenic coronaviruses. *Nat Rev Microbiol* 2019;17:181-192. PUBMED | CROSSREF
3. Hu B, Guo H, Zhou P, Shi ZL. Characteristics of SARS-CoV-2 and COVID-19. *Nat Rev Microbiol* 2021;19:141-154. PUBMED | CROSSREF

4. Dong W, Mead H, Tian L, Park JG, Garcia JI, Jaramillo S, Barr T, Kollath DS, Coyne VK, Stone NE, et al. The k18-human ace2 transgenic mouse model recapitulates non-severe and severe covid-19 in response to an infectious dose of the SARS-CoV-2 virus. *J Virol* 2022;96:e0096421. PUBMED | CROSSREF
5. Hijano DR, Brazelton de Cardenas J, Maron G, Garner CD, Ferrolino JA, Dallas RH, Gu Z, Hayden RT. Clinical correlation of influenza and respiratory syncytial virus load measured by digital PCR. *PLoS One* 2019;14:e0220908. PUBMED | CROSSREF
6. Chu CM, Poon LL, Cheng VC, Chan KS, Hung IF, Wong MM, Chan KH, Leung WS, Tang BS, Chan VL, et al. Initial viral load and the outcomes of SARS. *CMAJ* 2004;171:1349-1352. PUBMED | CROSSREF
7. Xu T, Chen C, Zhu Z, Cui M, Chen C, Dai H, Xue Y. Clinical features and dynamics of viral load in imported and non-imported patients with COVID-19. *Int J Infect Dis* 2020;94:68-71. PUBMED | CROSSREF
8. To KK, Tsang OT, Leung WS, Tam AR, Wu TC, Lung DC, Yip CC, Cai JP, Chan JM, Chik TS, et al. Temporal profiles of viral load in posterior oropharyngeal saliva samples and serum antibody responses during infection by SARS-CoV-2: an observational cohort study. *Lancet Infect Dis* 2020;20:565-574. PUBMED | CROSSREF
9. Dabisch PA, Biryukov J, Beck K, Boydston JA, Sanjak JS, Herzog A, Green B, Williams G, Yeager J, Bohannon JK, et al. Seroconversion and fever are dose-dependent in a nonhuman primate model of inhalational COVID-19. *PLoS Pathog* 2021;17:e1009865. PUBMED | CROSSREF
10. Ryan KA, Bewley KR, Fotheringham SA, Slack GS, Brown P, Hall Y, Wand NI, Marriott AC, Cavell BE, Tree JA, et al. Dose-dependent response to infection with SARS-CoV-2 in the ferret model and evidence of protective immunity. *Nat Commun* 2021;12:81. PUBMED | CROSSREF
11. McCray PB Jr, Pewe L, Wohlford-Lenane C, Hickey M, Manzel L, Shi L, Netland J, Jia HP, Halabi C, Sigmund CD, et al. Lethal infection of K18-hACE2 mice infected with severe acute respiratory syndrome coronavirus. *J Virol* 2007;81:813-821. PUBMED | CROSSREF
12. Winkler ES, Bailey AL, Kafai NM, Nair S, McCune BT, Yu J, Fox JM, Chen RE, Earnest JT, Keeler SP, et al. SARS-CoV-2 infection of human ACE2-transgenic mice causes severe lung inflammation and impaired function. *Nat Immunol* 2020;21:1327-1335. PUBMED | CROSSREF
13. Moreau GB, Burgess SL, Sturek JM, Donlan AN, Petri WA, Mann BJ. Evaluation of K18- hACE2 mice as a model of SARS-CoV-2 infection. *Am J Trop Med Hyg* 2020;103:1215-1219. PUBMED | CROSSREF
14. Yinda CK, Port JR, Bushmaker T, Offei Owusu I, Purushotham JN, Avanzato VA, Fischer RJ, Schulz JE, Holbrook MG, Hebner MJ, et al. K18-hACE2 mice develop respiratory disease resembling severe COVID-19. *PLoS Pathog* 2021;17:e1009195. PUBMED | CROSSREF
15. Yu G, Wang LG, Han Y, He QY. clusterProfiler: an R package for comparing biological themes among gene clusters. *OMICS* 2012;16:284-287. PUBMED | CROSSREF
16. Sturm G, Finotello F, List M. Immunedeconv: an R package for unified access to computational methods for estimating immune cell fractions from bulk RNA-sequencing data. *Methods Mol Biol* 2020;2120:223-232. PUBMED | CROSSREF
17. Bizzotto J, Sanchis P, Abbate M, Lage-Vickers S, Lavignolle R, Toro A, Olszevicki S, Sabater A, Cascardo F, Vazquez E, et al. SARS-CoV-2 infection boosts MX1 antiviral effector in COVID-19 patients. *iScience* 2020;23:101585. PUBMED | CROSSREF
18. Gusev E, Sarapultsev A, Solomatina L, Chereshnev V. SARS-CoV-2-specific immune response and the pathogenesis of COVID-19. *Int J Mol Sci* 2022;23:1716. PUBMED | CROSSREF
19. Wu D, Zhang R, Datta S. Unraveling T cell responses for long term protection of SARS-CoV-2 infection. *Front Genet* 2022;13:871164. PUBMED | CROSSREF
20. Rha MS, Jeong HW, Ko JH, Choi SJ, Seo IH, Lee JS, Sa M, Kim AR, Joo EJ, Ahn JY, et al. PD-1-expressing SARS-CoV-2-specific CD8+ T cells are not exhausted, but functional in patients with COVID-19. *Immunity* 2021;54:44-52.e3. PUBMED | CROSSREF
21. Kared H, Redd AD, Bloch EM, Bonny TS, Sumatoh H, Kairi F, Carbajo D, Abel B, Newell EW, Bettinotti MP, et al. SARS-CoV-2-specific CD8+ T cell responses in convalescent COVID-19 individuals. *J Clin Invest* 2021;131:e145476. PUBMED | CROSSREF
22. Takata H, Naruto T, Takiguchi M. Functional heterogeneity of human effector CD8+ T cells. *Blood* 2012;119:1390-1398. PUBMED | CROSSREF
23. Yamagata T, Benoist C, Mathis D. A shared gene-expression signature in innate-like lymphocytes. *Immunol Rev* 2006;210:52-66. PUBMED | CROSSREF
24. Iwata-Yoshikawa N, Uda A, Suzuki T, Tsunetsugu-Yokota Y, Sato Y, Morikawa S, Tashiro M, Sata T, Hasegawa H, Nagata N. Effects of Toll-like receptor stimulation on eosinophilic infiltration in lungs of BALB/c mice immunized with UV-inactivated severe acute respiratory syndrome-related coronavirus vaccine. *J Virol* 2014;88:8597-8614. PUBMED | CROSSREF

25. An D, Li K, Rowe DK, Diaz MC, Griffin EF, Beavis AC, Johnson SK, Padykula I, Jones CA, Briggs K, et al. Protection of K18-hACE2 mice and ferrets against SARS-CoV-2 challenge by a single-dose mucosal immunization with a parainfluenza virus 5-based COVID-19 vaccine. *Sci Adv* 2021;7:eabi5246. PUBMED | CROSSREF
26. Hama Amin BJ, Kakamad FH, Ahmed GS, Ahmed SF, Abdulla BA, Mohammed SH, Mikael TM, Salih RQ, Ali RK, Salh AM, et al. Post COVID-19 pulmonary fibrosis; a meta-analysis study. *Ann Med Surg (Lond)* 2022;77:103590. PUBMED | CROSSREF
27. Han X, Fan Y, Alwalid O, Li N, Jia X, Yuan M, Li Y, Cao Y, Gu J, Wu H, et al. Six-month follow-up chest CT findings after severe COVID-19 pneumonia. *Radiology* 2021;299:E177-E186. PUBMED | CROSSREF
28. Huang WJ, Tang XX. Virus infection induced pulmonary fibrosis. *J Transl Med* 2021;19:496. PUBMED | CROSSREF
29. Fernandez IE, Eickelberg O. New cellular and molecular mechanisms of lung injury and fibrosis in idiopathic pulmonary fibrosis. *Lancet* 2012;380:680-688. PUBMED | CROSSREF
30. Velardi E, Tsai JJ, van den Brink MR. T cell regeneration after immunological injury. *Nat Rev Immunol* 2021;21:277-291. PUBMED | CROSSREF
31. D'Abramo A, Vita S, Maffongelli G, Mariano A, Agrati C, Castilletti C, Goletti D, Ippolito G, Nicastri E; Spallanzani COVID-19 Case Investigation Team. Prolonged and severe SARS-CoV-2 infection in patients under B-cell-depleting drug successfully treated: a tailored approach. *Int J Infect Dis* 2021;107:247-250. PUBMED | CROSSREF